Experimental Identification of Downhill Protein Folding

Maria M. Garcia-Mira,[1,2*] Mourad Sadqi,[1] Niels Fischer,[1] Jose M. Sanchez-Ruiz,[2] Victor Muñoz[1†]

Theory predicts the existence of barrierless protein folding. Without barriers, folding should be noncooperative and the degree of native structure should be coupled to overall protein stability. We investigated the thermal unfolding of the peripheral subunit binding domain from *Escherichia coli*'s 2-oxoglutarate dehydrogenase multienzyme complex (termed BBL) with a combination of spectroscopic techniques and calorimetry. Each technique probed a different feature of protein structure. BBL has a defined three-dimensional structure at low temperatures. However, each technique showed a distinct unfolding transition. Global analysis with a statistical mechanical model identified BBL as a downhill-folding protein. Because of BBL's biological function, we propose that downhill folders may be molecular rheostats, in which effects could be modulated by altering the distribution of an ensemble of structures.

The accepted view in molecular and structural biology is that to perform their biological function, proteins must fold into unique three-dimensional structures, either spontaneously (*1*) or upon binding to their substrate (*2*). Accumulated experimental evidence indicates that folding proteins cross at least one free energy barrier (*3*). The existence of a barrier means that the mechanism of folding cannot be inferred directly from experiment and that folding kinetics must be interpreted by using, for example, linear free-energy relationships (*4*). On the other hand, the energy landscape theory predicts that under certain conditions, folding can proceed without crossing barriers (the downhill scenario) (*5*). In computer simulations, barrierless folding appears with very smooth stabilizing potentials (*6*). During downhill folding, all of the intermediate structures, and therefore the mechanism, are potentially observable (*7*). It has been argued that downhill folding can result in a nonexponential time course, especially if the roughness of the landscape increases as folding proceeds (*8*). Nonexponential kinetics have been recently observed when monitoring local relaxation dynamics on one side of the barrier for α-helix formation (*9*) and for folding (*10*, *11*). However, no examples have been identified of proteins that fold to a defined native structure without crossing any barriers.

We have recently established theoretically that the absence of barriers to folding is associated with a singular equilibrium behavior (*12*). For downhill folders, there is a unique thermodynamic state consisting of an ensemble of conformations that loses structure gradually as protein stability decreases. Therefore, a particularly useful strategy to identify downhill folding is to investigate protein unfolding at equilibrium with several techniques, each probing a different structural feature of the protein as it unfolds (*12*). In particular, we have investigated the unfolding of the peripheral subunit binding domain (PSBD) of the dihydrolipoamide succinyltransferase (the E2 subunit) from the 2-oxoglutarate dehydrogenase multienzyme complex of *Escherichia coli* (*13*). This domain is flanked by flexible linkers and connects the NH_2-terminal lipoyl and the COOH-terminal acyltransferase domains in the E2 subunit. It is ~40 residues long, comprising two parallel α helices connected by a long partially structured loop (*14*) (Fig. 1). PSBD is involved in regulating and coordinating the interplay between E2 and subunits E1 (2-oxoglutarate decarboxylase) and E3 (dihydrolipoamide dehydrogenase) (*15*). We produced the isolated PSBD (termed BBL) by chemical synthesis (*16*) and studied its thermal unfolding transition with three main techniques: differential scanning calorimetry (DSC) to directly measure the energetics of unfolding, far-ultraviolet (UV) circular dichroism (CD) to monitor the two α helices, and fluorescence resonance energy transfer (FRET) to investigate the end-to-end distance. BBL lacks natural fluorophores, so we introduced a naphthyl-alanine in the NH_2-terminus and a dansylated lysine in the COOH-terminus of the protein (Fig. 1). Because the fluorescence quantum yield of dansyl is very sensitive to the chemical environment, it provided a fourth probe of the structural integrity of BBL.

DSC experiments (*16*) done at pH 7.0 revealed a broad unfolding transition that spanned temperatures from below 280 K to 345 K (Fig. 2A). The absence of an initial baseline indicated that the distribution of populations was already changing even at the lowest temperatures explored. The DSC trace showed a clear maximum, which typically signals the transition midpoint temperature (T_m), at ~322 K. After crossing the T_m, the unfolding transition resumed more abruptly, resulting in an asymmetric DSC trace. Figure 2B shows the changes in FRET efficiency as temperature increased. Here, transfer efficiency was determined from the changes in the fluorescence quantum yield of both donor and acceptor (*16*). In experiments done at pH 7.0, the measured transfer efficiency was ~0.50 at the lowest temperatures. With an experimentally determined R_0 for the donor-acceptor pair and assuming an orientation factor (κ^2) of two-thirds (*16*), the observed transfer efficiency translated into an end-to-end distance of ~2.4 nm. This is in agreement with the distance calculated from the nuclear magnetic resonance (NMR) structure. The FRET efficiency sharply increased with temperature up to a value of ~0.73 at 320 K,

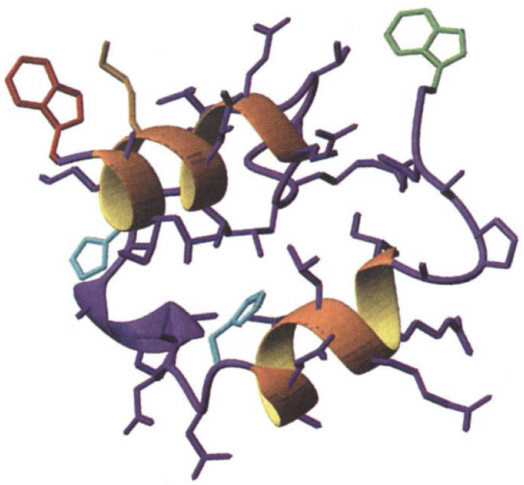

Fig. 1. The minimized average NMR structure of the BBL domain (Protein Data Bank accession number 1bbv.pdb). For clarity, the α helices are shown in a ribbon representation and in orange. Tryptophan residues were used in the model to signal the locations of the NH_2-terminal naphthyl-alanine (green) and COOH-terminal dansyl-lysine (red). Mutations of Ala_1 and Lys_{40} to Trp were carried out with the protein modeling program Whatif (*35*). The side chain of Lys_{36} is shown in orange to illustrate the interaction with the dansyl moiety, and the two histidines are shown in cyan.

[1]Department of Chemistry and Biochemistry and Center for Biomolecular Structure and Organization, University of Maryland, College Park, MD 20742, USA. [2]Departamento de Química-Física, Facultad de Ciencias, Universidad de Granada, Granada 18071, Spain.

*Present address: Biochemisches Laboratorium, Universität Bayreuth, D-95412 Bayreuth, Germany.
†To whom correspondence should be addressed. E-mail: vm48@umail.umd.edu

and then stabilized (Fig. 2B). The calculated end-to-end distance of BBL at the highest temperatures was ~1.9 nm: much shorter than the expected distance for a random walk chain of 40 residues, and even shorter than that for the native state. Therefore, thermally denatured BBL occurs in a somewhat collapsed form. This does not imply that BBL is more compact when denatured. In the native structure of BBL, the ends are placed at a distance of more than twice the radius of gyration (Fig. 1). However, unstructured heteropolymers can have large radii of gyration and short average end-to-end distances in the presence of attractive interactions (*17*). In BBL, these possibly are long-range electrostatic interactions between the charged NH_2- and COOH-terminal α helices. It appears that the thermal unfolding transitions uncovered by FRET and DSC are very different (*18*). The changes in end-to-end distance resumed even before the midpoint of the DSC transition was reached.

The fluorescence quantum yield of the COOH-terminal dansyl group as a function of temperature is shown in Fig. 2C. Dansyl fluorescence is mostly temperature-independent, so the changes observed at pH 7.0 for dansyl attached to BBL are due to perturbations in the local chemical environment induced by changes in protein structure (*19*). The fluorescence data showed no unfolding below 305 K. Above this temperature, the quantum yield started to decrease monotonically, but it did not reach a defined plateau even at the highest temperature explored (363 K). The far-UV CD spectrum of BBL at pH 7.0 and low temperature indicated a mixture of random coil and α-helix structure (Fig. 3A). The α-helix content estimated from the molar ellipticity at 222 nm is ~30%, in agreement with the average NMR structure. At high temperatures, the CD spectrum was characteristic of a denatured protein with some residual structure. The transition displayed an isodichroic point at ~203 nm but was wavelength-dependent (Fig. 3B). Singular-value decomposition (SVD) of the CD spectra at different temperatures rendered two main components (Fig. 3C). The first one corresponded to a CD spectrum of disordered structure and was mostly invariant with temperature. The second component had the features of an α helix. At pH 7.0, the amplitude of this component (Fig. 3C, inset) showed an unfolding transition with two phases. In the range from 280 to 315 K, a gradual decrease in α helix content was observed. A more pronounced unfolding process started at 315 K and was completed at 355 K. The low-temperature phase roughly coincided with the changes in FRET. However, the T_m for the second phase was ~8 K higher than the calorimetric T_m, but still lower than the T_m monitored by dansyl fluorescence. Comparison between the second SVD component and the basis CD spectra of α helices of varying length indicated that the average α-helix length was only about 5 residues (*16*). This result suggests that the α-helix signal of BBL decreases because of progressive shortening of the helices and not because of global unfolding.

BBL showed a very high sensitivity to acidic pH. Figures 2 (all panels) and 3A (inset) indicate that at pH 3.0, the protein was totally denatured. The DSC profile lacks any transition, and the heat capacity was substantially larger than at pH 7.0 and high temperature. The CD spectrum corresponds to a disordered structure at all temperatures, and the quantum yield of dansyl fluorescence was mostly invariant. Furthermore, the end-to-end distance determined by FRET was much larger at pH 3.0 than at pH 7.0. A pH titration of the thermal stability of BBL indicated that the midpoint for its pH-induced denaturation is ~5.0 (*20*). This can be explained by the protonation of two histidine residues that are placed at the hinges of the structure and are involved in many hydrophobic interactions (Fig. 1).

Thus, the equilibrium unfolding of BBL cannot be described as a simple two-state process. Global fits to a three-state model are not able to reproduce the experimental data either. The wavelength dependence and SVD analysis of the CD data indicate that BBL's α helices unraveled gradually. Together with the large spread of T_ms observed for different structural probes (from 295 to 335 K), this points to an unfolding process in which protein structure melts gradually. Similar behavior has been reported in the urea-induced unfolding of some molten globule states (*21*, *22*). However, high-resolution 2D NMR shows unambiguously that BBL has a defined 3D structure with specific tertiary contacts (fig. S1) (*23*). Nonconcerted unfolding starting from defined 3D structures is exactly what we expect for downhill folding (*12*).

To study the mechanism of nonconcerted unfolding, we have used a simple statistical mechanical model (*24*). Such models successfully describe the thermodynamics and kinetics of secondary structure formation and of important aspects of protein folding (*25*). For BBL, the model defined 821 species that correspond to all possible single stretches of native structure, from 0 to 40 nativelike residues. The thermodynamic properties of each species were calculated from the structure of the native fragment with a simple procedure

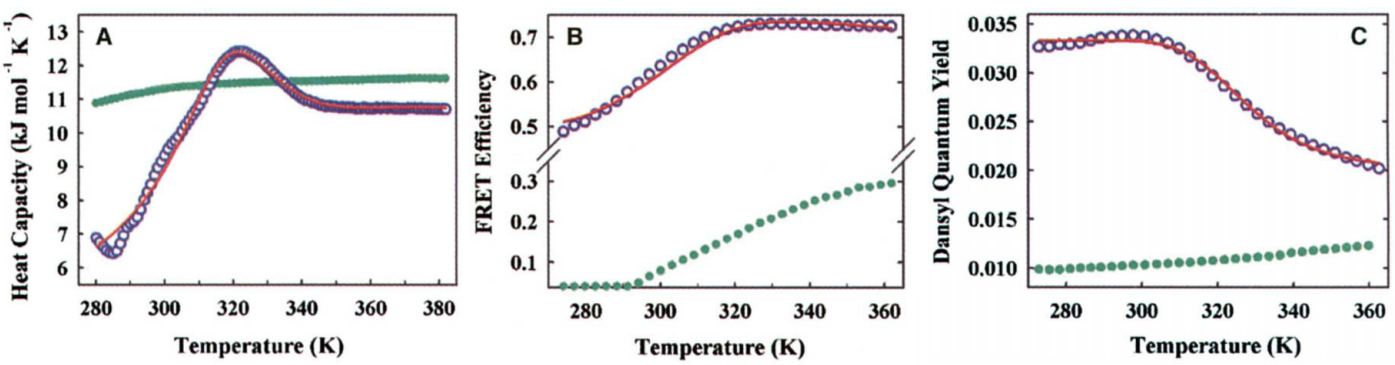

Fig. 2. (**A**) DSC of BBL. Absolute heat capacity is shown as a function of temperature for BBL at pH 7.0 (open blue circles) and pH 3.0 (solid green circles). The calculation of the absolute heat capacity for BBL at pH 7.0 with the statistical mechanical model and final parameters is shown as a solid red line. (**B**) FRET experiments in doubly labeled BBL. FRET efficiency is shown as a function of temperature for BBL at pH 7.0 (open blue circles) and pH 3.0 (solid green circles). Calculation of the FRET efficiency for BBL at pH 7.0 with the statistical mechanical model and final parameters is shown as a solid red line. The FRET efficiency of BBL at pH 3.0 was below the detection limit (<5%) in the range between 270 and 290 K. (**C**) Intrinsic fluorescence quantum yield of the COOH-terminal dansyl in doubly labeled BBL. The dansyl quantum yield is shown as a function of temperature for BBL at pH 7.0 (open blue circles) and pH 3.0 (solid green circles). Calculation of the dansyl quantum yield for BBL at pH 7.0 with the statistical mechanical model and final parameters is shown as a solid red line. The experiments in (B) and (C) were carried out (*16*) with sample concentrations of ~5 μM prepared in 20 mM buffer phosphate at pH 7.0 or 20 mM buffer glycine with hydrocloric acid at pH 3.0.

(*16*). With this scheme, four parameters were sufficient to describe the thermodynamics of the 821 species. This is only one more parameter than in the simplest two-state model. We fitted the model globally to all of the data by using a unique set of thermodynamic parameters and a series of basic rules to calculate spectroscopic properties from protein structure (*16*). The model reproduced all of the data very well [Figs. 2 (all panels) and 3D], and with reasonable parameters (*16*). Inspection of the changes in the distribution of probabilities for the 821 species as temperature increased revealed the landmark characteristic of downhill folding. At low temperatures, an ensemble of highly structured species dominated. As temperature increased, the ensemble broadened and shifted toward species with decreasing degrees of structure. However, even at high temperatures, a substantial amount of residual structure, localized primarily in the two α helices, was still present (Fig. 4). Calculation of the free energy as a function of the number of native residues produced barrierless profiles in which the position of the only minimum was correlated with overall stability (Fig. 4, insets). This behavior is intrinsic to the data, because the model produced free-energy barriers and definite intermediates when applied to two- and three-state proteins, respectively (*26*). Fits to a phenomenological 22-parameter three-state model in which the degree of structure for each state was allowed to vary with temperature reproduced the data well, but the final parameters resulted in a structurally continuous unfolding process.

BBL appears to be an example of downhill folding, confirming one of the most intriguing predictions of the energy landscape theory of protein folding (*5*). Our results suggest that all of the different stages in the folding reaction of BBL could be visited in equilibrium by simply modulating protein stability. Therefore, the application of high-resolution steady-state techniques, such as multidimensional NMR, should produce a description of BBL's unfolding process with high structural detail. Preliminary results from NMR experiments support this idea (*27*). The unfolding of a close relative of BBL, the PSBD from the pyruvate dehydrogenase complex of *Bacillus stearothermophilus*, has been described by Spector *et al.* as a two-state process with an apparent T_m of ~328 K (*28*). This conclusion was based on the spectroscopic investigation of the local environment of one tyrosine residue and single-wavelength far-UV CD experiments, which were analyzed with phenomenological baselines for the folded and unfolded states. However, from the line broadening of specific NMR signals, the same authors obtained a folding relaxation time of only ~45 μs (*29*), perhaps suggestive of barrierless folding (*30*). This highlights the importance of com-

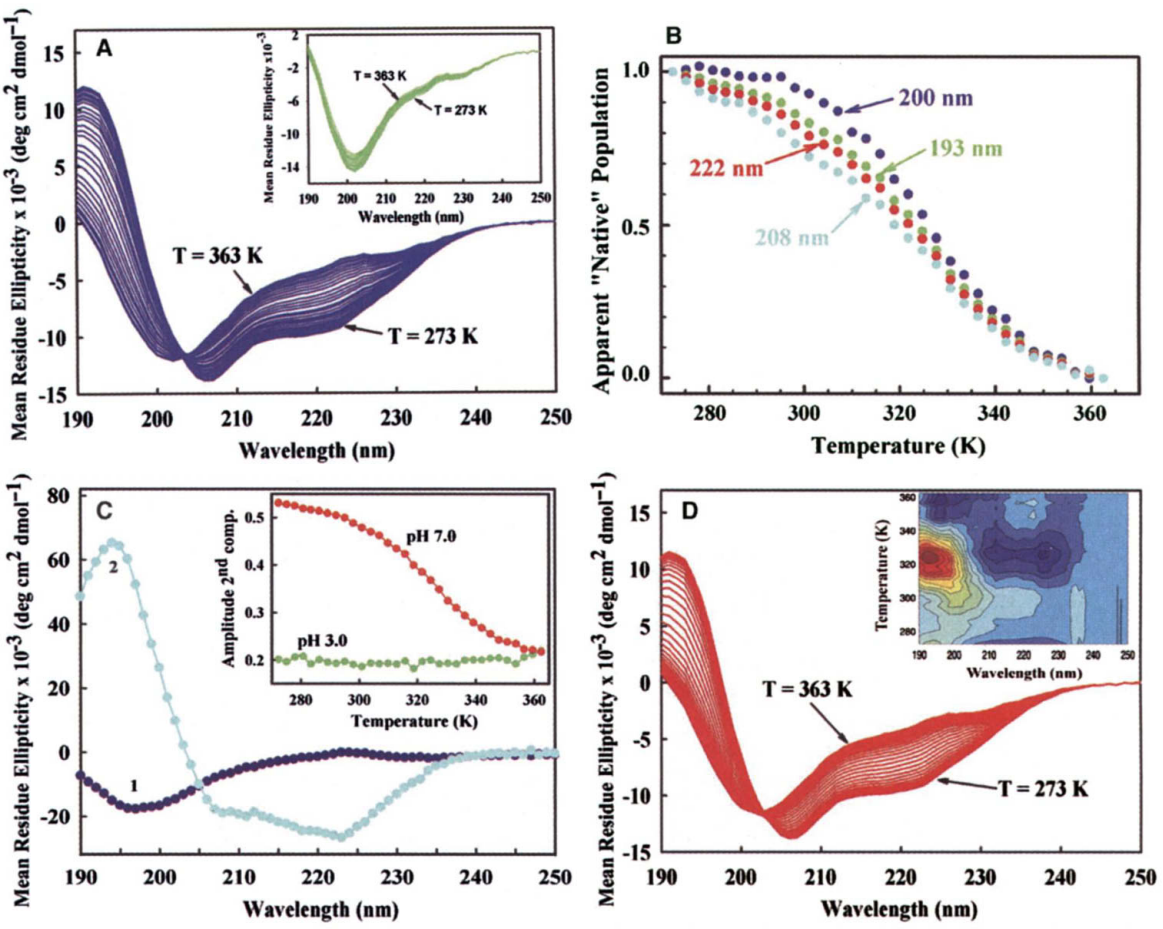

Fig. 3. Far-UV CD spectroscopy in BBL (**A**) Experimental far-UV CD of BBL as a function of temperature. Far-UV spectra were obtained every 3 K from ~273 to ~363 K (final cuvette temperatures were recorded with an external probe). The main figure shows in blue the 32 CD spectra at different temperatures and at pH 7.0. The inset shows in green the 32 CD spectra at similar temperatures but at pH 3.0. (**B**) Apparent unfolding transitions monitored by CD at different wavelengths. The curves are obtained by simple normalization of the raw CD data as a function of temperature, with the first point as 100% and the last point as 0%. (**C**) SVD of the combined temperature-dependent CD data at both pHs (7.0 and 3.0). Only the first (dark blue) and second (cyan) components are shown here, because all other components were noise. The components are displayed multiplied by their singular values to represent real CD spectra. The inset shows the amplitude vector for the second component of the experiments at pH 7.0 (red circles) and pH 3.0 (green circles). The amplitude of the first component was invariant with temperature. (**D**) Theoretical far-UV CD spectra of BBL as a function of temperature calculated with the statistical mechanical model and the final parameters obtained in the global fitting procedure. The main figure shows in red the 32 theoretical far-UV CD spectra of BBL at pH 7.0, calculated at the same temperatures as the experiment (Fig. 3A). The inset shows a contour map of the difference matrix between the 32 theoretical CD spectra and the 32 experimental CD spectra. In this map, dark red represents 1500 deg cm^2 dmol^{-1} and dark blue represents 500 deg cm^2 dmol^{-1}. Bright green corresponds to a value of 0 on this scale. The spectral region with the largest residuals corresponds to the deeper UV, in agreement with the fact that this is the region with higher experimental error. The experimental error estimated from all of the noise components (3rd to 32nd) obtained in the SVD procedure is ±1300 deg cm^2 dmol^{-1} at 190 nm, compared to ±420 deg cm^2 dmol^{-1} at 220 nm.

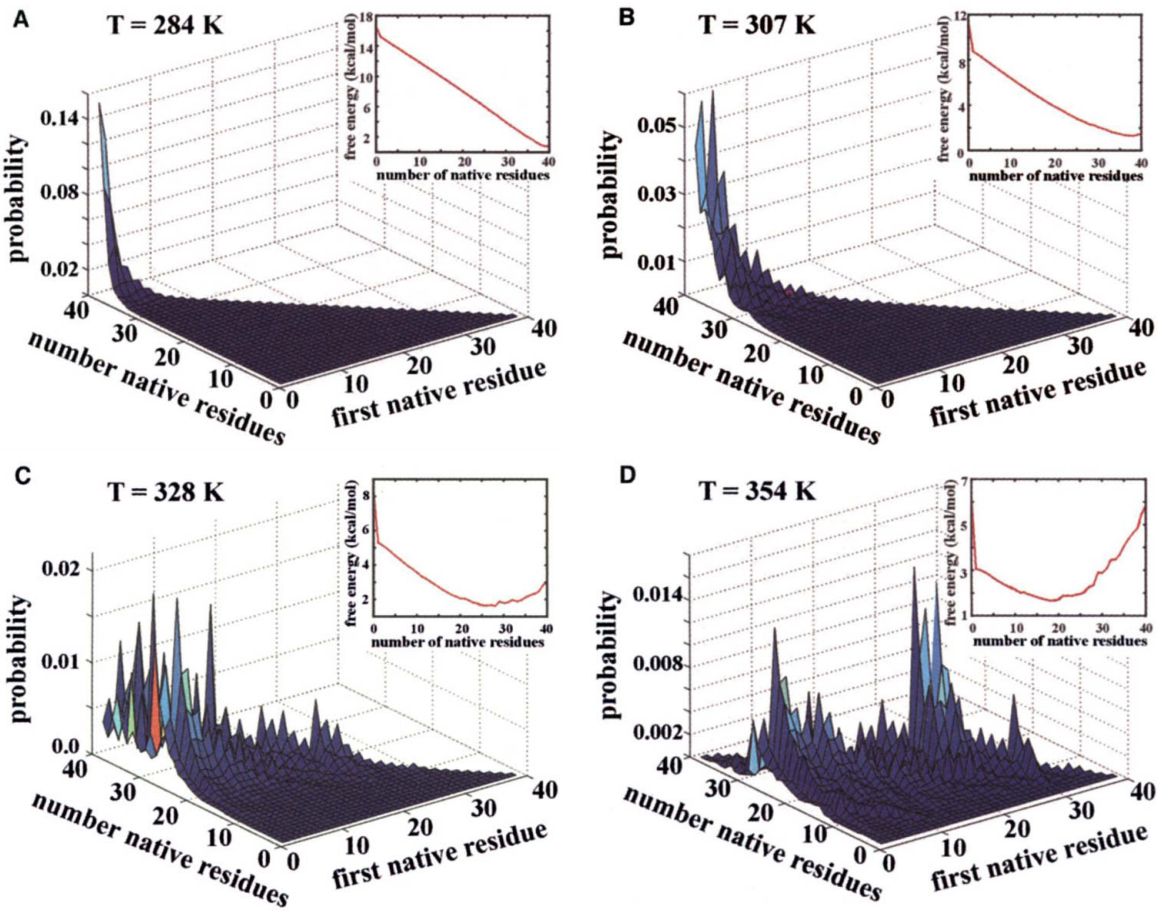

Fig. 4. The thermal unfolding process of BBL (**A** to **D**) The main panels show the probability distribution for the 820 structured species of BBL at various temperatures. The probabilities have been calculated with the statistical mechanical model and the parameters obtained from the global fitting to the DSC, FRET, dansyl fluorescence, and CD data. Each of the species is defined by two parameters: the position in the sequence of the first native residue and the length of the native stretch [such as (1, 40) for the fully folded state]. The population of the unfolded species (0,0) was below 0.1% at all temperatures. The insets show the free energy as a function of the number of native residues at the corresponding temperatures.

bining techniques that probe different structural features with a detailed analysis of the data to expose the complex equilibrium behavior inherent to downhill folding.

The rich conformational behavior of BBL could be exploited in protein regulation. In classical mechanisms, a two-state conformational change switches protein function on and off (*31*) or transmits a signal through quaternary interactions (*32*). For these phenomena to occur, the protein region involved in the conformational change must be flexible (*33*, *34*). In contrast to the binary character of switches, downhill-folding proteins can act as conformational rheostats. Downhill folders have global conformational fluctuations that, unlike those of natively unfolded proteins (*2*), are organized in hierarchical levels of structure. Therefore, a gradation in signal can be obtained by tuning the distribution of ensemble structures through binding to effectors or by modifying the environment with changes in pH or temperature. Additionally, the absence of barriers to folding could allow BBL to function as a molecular spring of adjustable length and stiffness. On the basis of these ideas, we can make experimentally testable predictions about how lypoic acid–dependent multifunctional enzymes coordinate the three subunits and channel the substrate (*15*). E2 subunits are modular, with three structurally independent domains. The PSBD in E2 may display conformational behavior similar to that of the isolated domain (BBL), because it is connected to the NH_2- and COOH-terminal domains by flexible linkers (*15*). The PSBD binds to E1 and E3 subunits and is postulated to be an important piece in the swinging arm mechanism. Synchronization of the three chemical reactions—decarboxylation, transacylation, and dehydrogenation—could be achieved by E1 and E3 subunits binding to different conformational subensembles of the PSBD. This requires that the PSBD conformational ensemble be poised to intermediate degrees of structure. In fact, BBL is partly unstructured at *E. coli*'s optimal growing temperature (310 K), whereas the isolated PSBD domain from *B. stearothermophilus* pyruvate dehydrogenase is near its unfolding midpoint at the optimal growing temperature of the thermophile *B. stearothermophilus* (323 to 333 K). Furthermore, the changes in end-to-end distance that occur in BBL in response to perturbations in its stability could dispense the mechanical force required to guide the swinging arm toward the active site of the COOH-terminal transacylase domain.

References and Notes

1. C. B. Anfinsen, *Science* **181**, 223 (1973).
2. K. Namba, *Genes Cells* **6**, 1 (2001).
3. S. E. Jackson, *Folding and Design* **3**, R81 (1998).
4. A. R. Fersht, A. Matouschek, L. Serrano, *J. Mol. Biol.* **224**, 771 (1992).
5. J. D. Bryngelson, J. N. Onuchic, N. D. Socci, P. G. Wolynes, *Proteins Struct. Funct. Genet.* **21**, 167 (1995).
6. C. Hardin, Z. Luthey-Schulten, P. G. Wolynes, *Proteins Struct. Funct. Genet.* **34**, 281 (1999).
7. W. A. Eaton, *Proc. Natl. Acad. Sci. U.S.A.* **96**, 5897 (1999).
8. N. D. Socci, J. Onuchic, P. G. Wolynes, *J. Chem. Phys.* **104**, 5860 (1996).
9. C. Y. Huang *et al.*, *Proc. Natl. Acad. Sci. U.S.A.* **99**, 2788 (2002).
10. J. Sabelko, J. Ervin, M. Gruebele, *Proc. Natl. Acad. Sci. U.S.A.* **96**, 6031 (1999).
11. D. T. Leeson, F. Gai, H. M. Rodriguez, L. M. Gregoret, R. B. Dyer, *Proc. Natl. Acad. Sci. U.S.A.* **97**, 2527 (2000).
12. V. Muñoz, *Int. J. Q. Chem.* **90**, 1522 (2002).
13. L. C. Packman, R. N. Perham, *FEBS Lett.* **206**, 193 (1986).
14. M. A. Robien *et al.*, *Biochemistry* **31**, 3463 (1992).
15. R. N. Perham, *Annu. Rev. Biochem.* **69**, 961 (2000).
16. Materials and methods are available as supplementary material on *Science* Online.
17. D. Thirumalai, D. Klimov, R. I. Dima, *Adv. Chem. Phys.* **120**, 35 (2002).
18. The differences observed in the thermal unfolding of BBL when monitored by DSC and FRET are not a consequence of the incorporation of the dansyl group in the COOH-terminus of the protein for the FRET experiments. The thermal unfolding of BBL monitored by far-UV CD and analyzed by SVD (Fig. 3) is identical for the two variants of BBL, with and without the dansyl group. This result is further supported by DSC experiments of dansylated BBL in dilute solutions (25 μM) and nondansylated BBL at standard DSC concentrations (0.25 mM). (The higher overall hydrophobicity of dansylated BBL results in

high-temperature–induced aggregation at the standard DSC concentrations.)
19. The COOH-terminal dansyl-lysine is placed at the end of the second α helix of BBL. Therefore, in the completely folded structure, the dansyl moiety is in relative proximity to the side chain of Lys_{36} (Fig. 1). In principle, in this configuration the intrinsic quantum yield of dansyl could be quenched by a proton transfer reaction from the protonated ε-amino group of Lys_{36}. Furthermore, the structure of BBL reveals a partially solvent-exposed hydrophobic core formed by inefficient packing between the two helices. A dansyl group hanging from a partially unfolded COOH-terminal tail can experience transient interactions with this core that will increase its quantum yield by effectively decreasing the average polarizability of its environment. These transient interactions between the dansyl group and the protein are sufficient to perturb its fluorescence quantum yield but do not substantially modify the energetics of BBL's unfolding (*18*).
20. M. M. Garcia-Mira, B. Ibarra-Molero, J. M. Sanchez-Ruiz, V. Muñoz, in preparation.
21. B. A. Schulman, P. S. Kim, C. M. Dobson, C. Redfield, *Nature Struct. Biol.* **4**, 630 (1997).
22. A. K. Chamberlain, S. Marqusee, *Biochemistry* **37**, 1736 (1998).
23. The 1D H^1 NMR spectrum of BBL at 293 K is well resolved and has large signal dispersion in the amide region [7.3 to 9.1 parts per million (ppm)], signaling a protein with defined 3D structure (fig. S1A). The 2D H^1 NMR analysis confirms this conclusion. Double-quantum filtered correlation, total correlation, and nuclear Overhauser effect (NOE) spectroscopy experiments produce 2D spectra with sharp cross peaks and little spectral overlap (fig. S1, B through E). All expected H^1 signals have been identified and assigned with the standard sequential procedure. The chemical shifts measured in our BBL construct coincide with those previously reported in a longer variant for which the high-resolution 3D structure has been determined (*14*). Differences in chemical shifts >0.1 ppm are only found for residues with ionizable groups or their sequence neighbors. These are most likely due to small pH discrepancies between the two experiments. Series of sequential NH–NH (i,i + 1) NOEs are clearly observed for residues in the NH_2- and COOH-terminal regions, indicating that the expected α helices are present (fig. S1D). Hδ-Hδ long-range NOEs that correspond to specific tertiary contacts in the native structure are also clearly observed (fig. S1E).
24. The model applied in this work is very similar to the one described previously by Muñoz & Eaton (*32*). The main statistical difference lies in the use of residues, instead of peptide bonds, as conformational units. The partition function has been truncated according to the single sequence approximation, as previously described (*33*). Under this approximation, the number of species in the model reduces to the total number of single stretches of native structure plus the random coil. Each species in the model is identified by two parameters: the position in the sequence of the first native residue and the number of residues in the native stretch [such as (1,40) for the fully native structure]. This approximation is quite accurate for calculating thermodynamic properties.
25. V. Muñoz, *Curr. Opin. Struct. Biol.* **11**, 212 (2001).
26. V. Muñoz, W. A. Eaton, *Proc. Natl. Acad. Sci. U.S.A.* **96**, 11311 (1999).
27. M. Sadqi, V. Muñoz, unpublished data.
28. S. Spector *et al.*, *J. Mol. Biol.* **276**, 479 (1998).
29. S. Spector, D. P. Raleigh, *J. Mol. Biol.* **293**, 763 (1999).
30. S. J. Hagen, J. Hofrichter, A. Szabo, W. A. Eaton, *Proc. Natl. Acad. Sci. U.S.A.* **93**, 11615 (1996).
31. M. V. Milburn *et al.*, *Science* **247**, 939 (1990).
32. M. Perutz, *Nature* **228**, 726 (1970).
33. M. Young, K. Kirshenbaum, K. A. Dill, S. Highsmith, *Protein Sci.* **8**, 1752 (1999).
34. E. Freire, *Proc. Nat. Acad. Sci. U.S.A.* **97**, 11680 (2000).
35. Whatif for Windows, G. Vriend, *J. Mol. Graph.* **8**, 52 (1990).
36. We thank B. Ibarra-Molero for collaborating in the data analysis and G. Lorimer for helpful suggestions on the manuscript. V.M. is a recipient of a Dreyfus New Faculty Award, a Packard Fellowship for Science and Engineering, and a Searle Scholar Award. The research described in this article has been supported in part by grant 36601–AC4 from the Petrol Research Fund (V.M.) and grant BIO2000–1437 from the Spanish Ministry of Science and Technology (J.M.S.R.).

Supporting Online Material
www.sciencemag.org/cgi/content/full/298/5601/2191/DC1
Materials and Methods
Figs. S1 and S2
References and Notes

27 August 2002; accepted 16 October 2002

Evidence for Antibody-Catalyzed Ozone Formation in Bacterial Killing and Inflammation

Paul Wentworth Jr.,[1] Jonathan E. McDunn,[1] Anita D. Wentworth,[1] Cindy Takeuchi,[2] Jorge Nieva,[3] Teresa Jones,[1] Cristina Bautista,[1] Julie M. Ruedi,[3] Abel Gutierrez,[3] Kim D. Janda,[1] Bernard M. Babior,[3] Albert Eschenmoser[1,4] Richard A. Lerner[1]

Recently, we showed that antibodies catalyze the generation of hydrogen peroxide (H_2O_2) from singlet molecular oxygen ($^1O_2$*) and water. Here, we show that this process can lead to efficient killing of bacteria, regardless of the antigen specificity of the antibody. H_2O_2 production by antibodies alone was found to be not sufficient for bacterial killing. Our studies suggested that the antibody-catalyzed water-oxidation pathway produced an additional molecular species with a chemical signature similar to that of ozone. This species is also generated during the oxidative burst of activated human neutrophils and during inflammation. These observations suggest that alternative pathways may exist for biological killing of bacteria that are mediated by potent oxidants previously unknown to biology.

A central concept of immunology is that antibodies perform the sole function of marking antigens for destruction by effector systems such as complement and phagocytic cells (*1*). Work on antibody catalysis has demonstrated that the antibody molecule is capable of carrying out highly sophisticated chemistry, although there has been no direct evidence that this catalytic potential is used in nature (*2*). This view is consistent with the known organization of the humoral immune system, in that simple antigen binding is sufficient to activate more sophisticated effector systems and, thus, killing of pathogens can be achieved without the need to invoke any chemistry within the antibody molecule itself. Recently however, we found that all antibodies, regardless of source or antigenic specificity, can catalyze redox chemistry that is independent of antibody binding (*3*) and appears to be highly analogous to that carried out by the effector mechanism of phagocytic cells (*4*). When exposed to singlet molecular oxygen ($^1O_2$*), antibodies oxidize water to produce H_2O_2 via the postulated intermediacy of H_2O_3 (*5*). In the present study, we examined whether this pathway might play any role in immune protective function of antibodies against bacteria and in inflammation.

Initial bactericidal studies focused on the gram-negative bacteria *Escherichia coli* (XL1-blue and O-112a,c) (*6*). Given the known bactericidal action of $^1O_2$* itself (*7*), these studies required a $^1O_2$* generating system that would not, on its own, kill *E. coli* (*8*) but would activate the water-oxidation pathway of antibodies. Negligible bactericidal activity against the two *E. coli* serotypes (~10^7 cells/ml) was observed when hematoporphyrin IX (HPIX, 40 μM), an efficient sensitizer of $^3O_2$ (*9*), was irradiated with white light (light flux 2.7 mW cm^{-2}) for 1 hour in phosphate buffered saline (PBS, pH 7.4) at 4° ± 1°C. However, addition of antigen-specific or nonspecific monoclonal antibodies (20 μM) to this system resulted in killing of >95% of the bacteria (Fig. 1A) (*6*). This bactericidal action seems to be a general property of antibodies, in that regardless of origin or antigen specificity, all antibodies display this activity. This bactericidal activity was a function of antibody concentration (Fig. 1B), irradiation time (Fig. 1C), and HPIX concentration (at a given light flux) (Fig. 1D). These obser-

[1]Department of Chemistry, [2]Department of Immunology, [3]Department of Molecular and Experimental Medicine and The Skaggs Institute for Chemical Biology, The Scripps Research Institute, 10550 North Torrey Pines Road, La Jolla, CA 92037, USA. [4]Laboratorium für organische Chemie, Eidgenössichsche Technische Hochschule (ETH) Hönggerberg HCl-H309, Universitaetstrasse 16 CH-8093 Zürich, Switzerland.